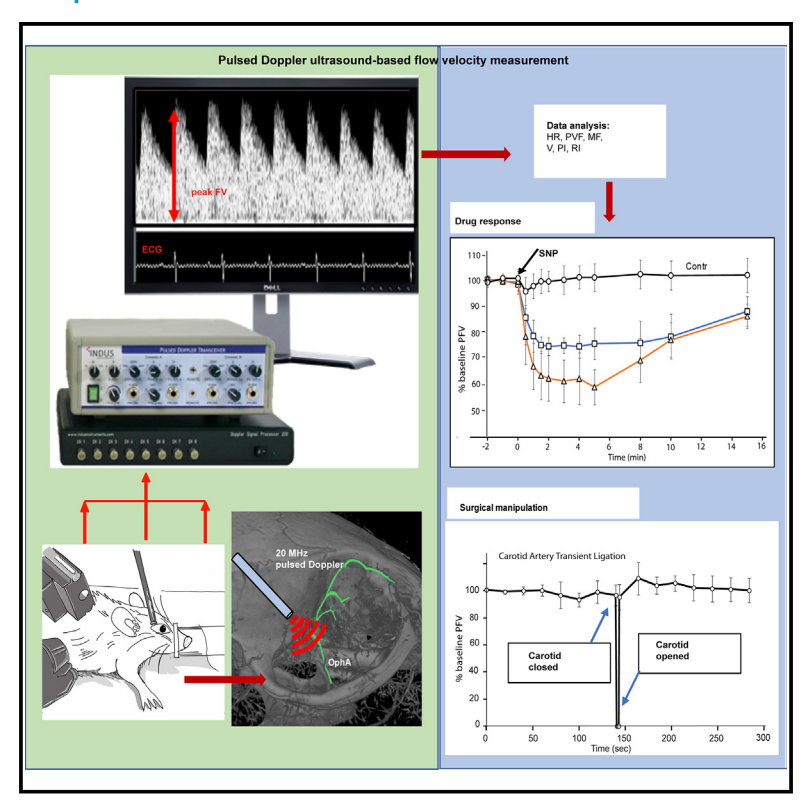
# Non-invasive real-time pulsed Doppler assessment of blood flow in mouse ophthalmic artery

### **Graphical abstract**



### **Authors**

Iraida Sharina, Radwa Awad, Soren Cobb, Emil Martin, Sean P. Marrelli, Anilkumar K. Reddy

### Correspondence

iraida.g.sharina@uth.tmc.edu

### In brief

Sharina et al. developed a Doppler ultrasound method that provides a non-invasive measurement of blood flow velocity in the mouse ophthalmic artery (OphA). The method can be used for the specific evaluation of the OphA function or as a surrogate approach to study cerebral arteries deriving from the internal carotid artery.

### **Highlights**

- Non-invasive Doppler ultrasound for measurement of blood flow velocity in mouse OphA
- Real-time and high-resolution measurements for acute or longitudinal studies
- Functional validation of method with pharmacological and surgical manipulations
- Application to blood flow regulatory mechanisms or pharmacological screening studies







### Report

# Non-invasive real-time pulsed Doppler assessment of blood flow in mouse ophthalmic artery

Iraida Sharina, 1,5,\* Radwa Awad, 1 Soren Cobb, 1 Emil Martin, 1 Sean P. Marrelli, 2 and Anilkumar K. Reddy3,4

\*Correspondence: iraida.g.sharina@uth.tmc.edu https://doi.org/10.1016/j.crmeth.2025.100983

**MOTIVATION** The ophthalmic artery (OphA) is essential for the health of the eye, and compromised blood flow in the OphA is a critical contributor to various eye pathologies. However, there is currently a lack of direct, non-invasive methods to measure OphA blood flow. The method we present allows a non-invasive assessment of blood flow parameters in the OphA at its point of emergence from the cranium and into the orbit. This approach enables longitudinal experiments in the same animal and eliminates the need for invasive procedures to assess the OphA in mice. The high time resolution, accuracy, and reproducibility of the presented approach, combined with reduced data variability, enable the characterization of the kinetics of drug responses with previously unmatched temporal resolution.

### **SUMMARY**

Non-invasive and high-temporal resolution methods for characterizing blood flow in mouse cranial arteries, such as the ophthalmic artery (OphA), are lacking. We present an application of pulsed Doppler ultrasound to provide real-time, non-invasive measurement of blood flow velocity in the OphA through an identified soft tissue window in the mouse head. We confirmed the identity of the artery and mapped its origin from the internal carotid artery by a combination of microcomputed tomography (microCT) vascular imaging and transient occlusion of the internal carotid artery. Application of our approach demonstrated sex differences in the OphA vasodilative response to agonists. We also evaluated real-time flow characteristics in the OphA in response to transient carotid artery ligation. The method will provide a simple and low-cost approach for screening drugs targeting ophthalmic blood flow and can be used as a more accessible surrogate of cerebral blood flow in both acute and longitudinal imaging studies.

### **INTRODUCTION**

Rodent genetic and disease models are of major importance in preclinical cerebrovascular research, <sup>4</sup> as they can be manipulated with a wide array of tools targeting specific genes in diverse pathological contexts. The high similarity between mice and human blood velocity magnitudes and waveforms simplifies the translation of collected knowledge to human therapies. <sup>5</sup> Multiple techniques have been developed to assess cranial blood flow velocity, such as intravascular implanted sensors, X-ray imaging, nuclear and magnetic resonance imaging, thermal diffusion, and optical and ultrasound techniques. <sup>6</sup> Non-invasive methods play a special role in the assessment of cerebrovascular function *in vivo*. <sup>6</sup> The non-invasive Doppler technique adapted for blood flow velocity measurements in various mouse vascular beds is convenient and easy to apply for the characterization of vascular

function in mouse models of aging, vascular remodeling, and the effects of surgical or pharmacological interventions. <sup>7–10</sup> The recent development of high-frequency ultrasound Doppler adapted for non-invasive measurements of blood flow velocity in small rodents has been a valuable addition to the set of tools facilitating the translation of murine studies to human physiology. <sup>11–14</sup>

Transcranial Doppler (TCD) ultrasound is routinely used to evaluate human cerebral blood flow (CBF) under various conditions. TCD sonography provides rapid, non-invasive, and real-time measurements of large intracranial blood vessels and is widely used in clinical and preclinical studies with human and large primate subjects.  $^{15,16}$  Low-frequency ( $\leq 2$  MHz) ultrasound signals penetrate the skull bone and provide an accurate measurement of the blood flow and vascular reactivity in selected cranial blood vessels. For example, TCD is used to assess the



<sup>&</sup>lt;sup>1</sup>Cardiology Division, Department of Internal Medicine, The University of Texas-McGovern Medical School, Houston, TX 77054, USA

<sup>&</sup>lt;sup>2</sup>Department of Neurology, The University of Texas-McGovern Medical School, Houston, TX 77030, USA

<sup>&</sup>lt;sup>3</sup>Section of Cardiovascular Research, Department of Medicine, Baylor College of Medicine, Houston, TX 77030, USA

<sup>&</sup>lt;sup>4</sup>Indus Instruments, Webster, TX 77598, USA

<sup>&</sup>lt;sup>5</sup>Lead contact



blood flow in major cerebral vessels to evaluate the risk of stroke in children diagnosed with sickle cell disease. 17 However, to resolve spatial and temporal resolutions for blood flow recordings in mice, which have significantly higher heart rates (>400 beats per min) and much smaller vessel diameters, a high-frequency transducer (10-20 MHz) is required. 18,19 The higher-frequency 20-MHz pulsed Doppler probe enables data sampling at rates with sufficient frequency and temporal resolution for mice, 19 allowing the determination of blood flow parameters and measures of vascular reactivity in real time in mice. The drawback, however, is that the higher-frequency ultrasound waves are more easily absorbed by tissue,<sup>20</sup> cannot penetrate the skull bone, 15,17 and become distorted, thus deteriorating the measurement quality.<sup>21</sup> To overcome this limitation, a partial or full craniotomy is often performed. 22,23 This invasive approach may alter cerebral vascular responses due to inflammation, gliosis, changed intracranial pressure, or local heating due to the skull thinning procedure. 23,24 Creating a cranial window requires skilled surgical personnel and extended post-surgery recovery times.<sup>25,26</sup>

The goal of this study was to develop a non-invasive Doppler approach that assesses mouse cranial arterial blood flow in studies of cerebrovascular regulation. We present a new adaptation of conventional pulsed Doppler flow velocity measurement that offers a non-invasive, direct, and real-time assessment of blood flow velocity in the mouse OphA. We identified and validated a unique soft tissue window at the temporal canthus of the mouse eye, which is unobstructed by the orbital bone. We confirmed that the OphA, derived from the internal carotid artery (ICA), is indeed the target for the ultrasound probe. We also present an effective application of our method in two highly relevant cerebrovascular experimental settings: when blood flow is (1) modulated pharmacologically or (2) manipulated mechanically. Our method avoids surgical intervention for assessing hemodynamic parameters of the OphA blood flow and enables longitudinal and repetitive experiments on the same animal. We believe that our approach will facilitate the research of vascular abnormalities in ocular disease by simplifying acute and longitudinal studies in the OphA. In addition, important similarities with cerebral vasculature and a direct connection to the ICA make studies in the OphA relevant for surrogate assessment of cerebrovascular pathological mechanisms in various disease states.

### **RESULTS**

### The orbital opening in mice provides a window for noninvasive pulsed Doppler access to ocular arterial blood flow

We aimed to identify and validate a previously unexplored anatomical location on the mouse head for non-invasive assessment of cranial blood flow using a non-imaging Doppler ultrasound. Literature analysis did not yield a Doppler application for mouse intracranial blood flow velocity measurements that did not require the removal or thinning of the skull. <sup>22,23</sup> We reviewed anatomical atlases, looking for a natural opening on the skull that exposes intracranial arteries. The orbital opening, where several intracranial arteries reside, was deemed promising.

To assess the blood flow dynamics, we used the ultrasound-based Doppler flow velocity measurement system (DFVS) previously developed to characterize vascular physiology in mice. <sup>19,27</sup> The experimental setup consists of 10/20-MHz ultrasonic transducers; analog electronics for Doppler blood flow velocity measurement, signal acquisition, and processing; and dedicated software for real-time display and offline analysis (Figure 1). The 20-MHz pulsed Doppler probe used in the current study has a small diameter (2.25 mm), allowing for ample flexibility and maneuverability in the orientation of the probe and the ultrasound beam. <sup>14,28</sup>

Guided by the real-time display of the waveform, we scanned the surface of the eyeball and the region around the eyeball in the orbital opening with the US probe, searching for the optimal position of the probe that provided the strongest signal for arterial blood flow, as described in the STAR Methods section. We found that the position near the temporal cantus of the eye produces a waveform characteristic for arterial blood flow (Figure 1) highly similar to the Doppler signal of a human eye artery. Figure S1 displays examples of optimal, suboptimal, and unacceptable spectral waves for comparison. The blood flow velocity waveform was suitable for the extraction of several parameters, including the peak, mean, and minimum blood flow velocities (Table 1). Regional cerebral impedance could be calculated using the angle-independent pulsatility index (PI = (Vpeak - Vmin)/ Vmean) and resistivity index (RI = (Vpeak - Vmin)/Vpeak).<sup>29</sup> All parameters are relevant for the characterization of the vascular function of ophthalmic and cerebral arteries in mouse models.8

### Localization of targeted artery by microCT imaging

To determine the identity of the artery producing the signal, we employed microcomputed tomography (microCT) imaging to correlate the target path of the ultrasound probe with the underlying skull and vascular anatomy (see STAR Methods). After a characteristic Doppler signal from the targeted artery was obtained (Figure 1, inset), a needle was inserted along the path of the probe to a 0.5 cm depth and secured in place. The three-dimensional (3D) images of the head with and without the fiduciary needle (Figures 2A and 2B; Video S1) were then used to extrapolate the location of the probe relative to the cranial vasculature by comparing it to a 3D microCT with arterial vascular contrast (Vascupaint). The location of the US probe (Figure 2C) correlates with the OphA at its point of emergence from the optic canal as the source of the acquired Doppler signal.

# In vivo microCT imaging with vascular contrast agent confirms the OphA as the targeted artery originating from the ICA

In vivo microCT imaging enhanced by the blood pool contrast agent (VivoVist) determined that there was a single artery of a sufficient size and orientation capable of generating the observed ultrasound signal (Figure 2D). The artery, which emerged from the skull through the optic canal, was traced distally and proximally to confirm its identity as the OphA. Tracing to its upstream source revealed that the OphA originates as an early branch of the ICA. The OphA quickly enters the tympanic bulla and then runs alternately above and below the sphenoid bone before its final exit of the cranium via the optic canal





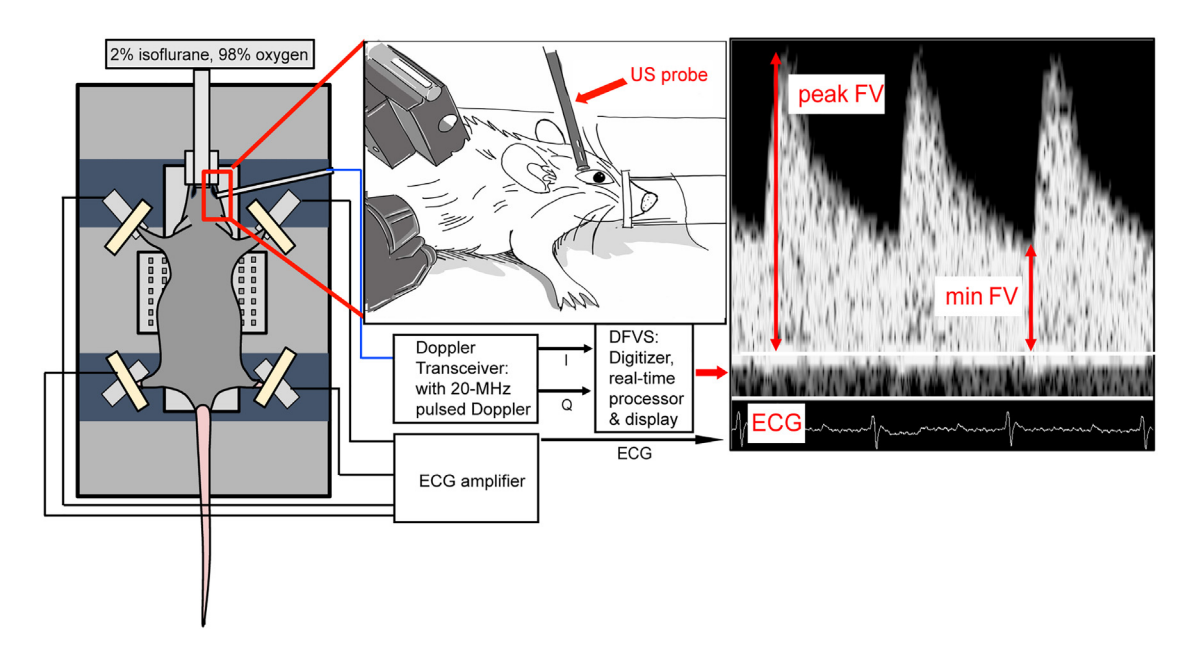


Figure 1. Setup of non-invasive Doppler OphA blood flow velocity measurements at mouse orbital opening

An anesthetized mouse is placed in a prone position on the ECG board. The Doppler probe sensor tip is at the temporal canthus (left and center). Doppler in-phase (I), quadrature (Q), and ECG signals are acquired, processed, displayed, and recorded in real-time (middle). Doppler velocity signal waveforms with major parameters are acquired for analysis (right). DVFS, Doppler flow velocity system; US, ultrasound; ECG, electrocardiogram; FV, flow velocity.

(Figures 2D–2F). Within the base of the cranium, the OphA travels parallel to the ICA within the circle of Willis (Figure 2E), sometimes fully within the cranium and sometimes traversing beneath the sphenoid bone (Figure 2F). Higher-resolution ex vivo microCT imaging using vascular contrast perfusion (Vascupaint) shows distal branching of this emerging segment into various known branches of the OphA (Figure 2C).

# Surgical validation of the targeted OphA as a branch of the ICA

To provide functional confirmation of our anatomical findings, we recorded the OphA Doppler signal while alternately occluding the ICA or the external carotid artery (ECA) (Figure 3), as described in the STAR Methods. Since the OphA branches off

the ICA, OphA flow should drop when the ICA, but not the ECA, is occluded. After a stable Doppler baseline flow was established (Figure 3D), the ECA and ICA were sequentially transiently occluded. Only occlusion of the ICA caused the loss of blood flow (Figure 3D), consistent with the anatomical-based assignment with microCT.

### **OphA** vasoreactivity response to SNP

Acetylcholine-induced and endothelium-dependent vasodilation of mouse retinal arterioles and OphA is mediated predominantly by endothelial nitric oxide (NO) synthase.<sup>30,31</sup> To validate our method in pharmacological studies, we examined the effect of a commonly used NO-generating vasodilator (sodium nitroprusside [SNP]) on mean systemic blood pressure (BP) and the blood

Table 1. OphA blood flow parameters acquired and calculated by the Doppler system

	3 min post-injection			t test, p value		
	Control, average ± SD	Males, average ± SD	Females, average ± SD	Males versus controls	Females versus controls	Males versus females
Heart rate (beats/min)	487 ± 44	558.9 ± 42	506.3 ± 31	0.02271	0.43678	0.07
Peak velocity (cm/s)	22.1 ± 2	$16.8 \pm 1.5$	$12.9 \pm 3.4$	0.00313	0.00071	0.07
Peak velocity (% of BL PFV)	100.1 ± 5	75.1 ± 2	61.5 ± 8.1	0.00001	0.00001	0.03
Mean flow velocity (cm/s)	$16.9 \pm 2.1$	$10.4 \pm 1.2$	$7.9 \pm 2.4$	0.00020	0.00009	0.13
Pulsatility index	$0.5 \pm 0.04$	$0.91 \pm 0.2$	$1.0 \pm 0.4$	0.00250	0.02361	0.62
Resistivity index	$0.38 \pm 0.1$	$0.55\pm0.1$	$0.57 \pm 0.1$	0.00134	0.00134	0.76

Absolute values for heart rate and PFV acquired 3 min post-SNP injection in control, male, and female experimental groups (n = 5 each) are presented. Mean flow velocity and pulsatility and resistivity indexes are shown. Changes in the PFV calculated as a percentage of baseline flow for each animal are indicated. Averages, standard deviations (SDs), and p values for comparisons between different groups are presented.



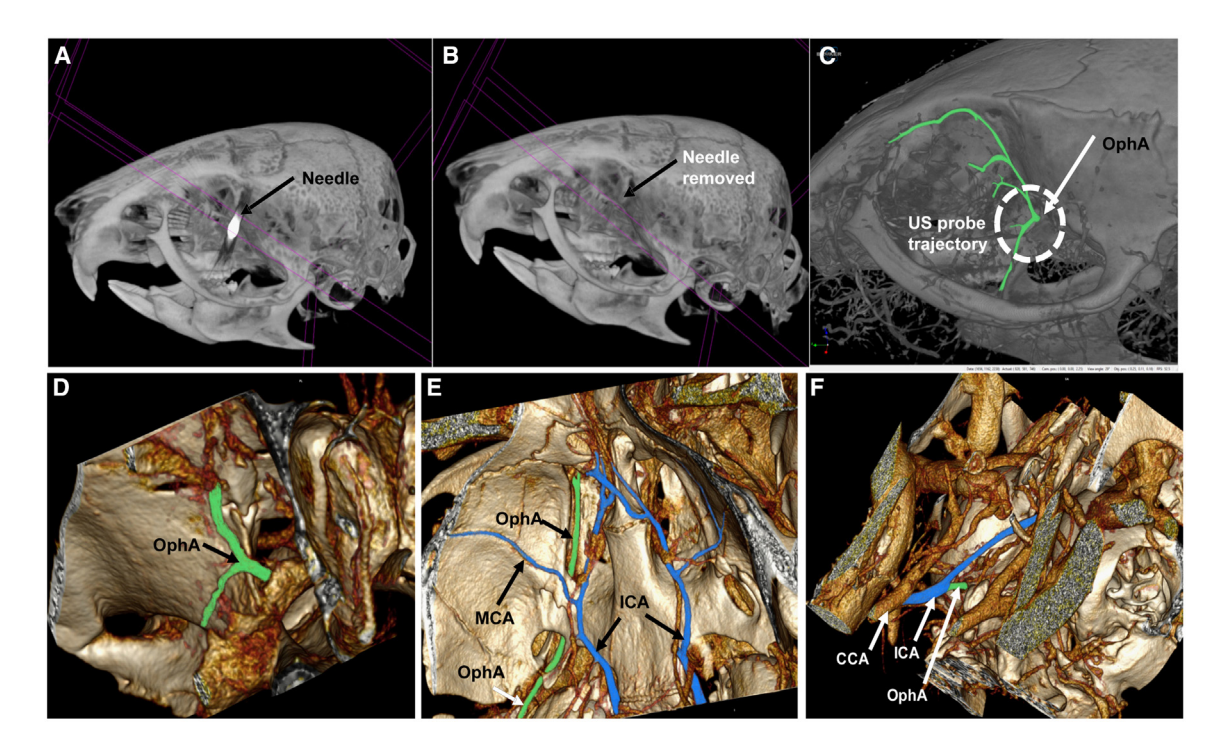


Figure 2. Defining the ultrasound probe signal trajectory by microCT

(A and B) Mouse skull images with the fiduciary needle in place (A) and after removal (B).

(C) MicroCT imaging of a mouse following transcardiac perfusion with Vascupaint to visualize the arterial vasculature. The white dashed circle indicates the region targeted by the ultrasound probe. OphA indicates the ophthalmic artery is emerging from the optic canal.

(D–F) In vivo microCT vascular tracing of the OphA from its origin off the proximal internal carotid artery (ICA) to its emergence into the orbit. (D) View into the orbit from outside the skull. (E) View from superior aspect showing OphA path, circle of Willis, and major branches. (F) View from inferior aspect showing the origin of the OphA from the ICA. The OphA is color coded in green and the ICA and branches of the circle of Willis are in blue. CCA, common carotid artery.

flow velocity in the OphA. Male (M) and female (F) mice were injected with SNP (1 mg/kg, intraperitoneal [i.p.]) or PBS. OphA's blood flow waveforms were recorded at different time points following SNP injection (Figures 4A and 4B) and plotted as a percentage of change in the peak blood flow velocity (PFV) from the initial baseline (Figure 4B). PFV demonstrated that SNP decreases the PFV by up to 28.6%  $\pm$  7.6% in males and 38.3%  $\pm$ 6.7% in females versus the control group (C). The maximal response of OphA PFV occurred 5 min post-injection, while full recovery was reached 30 min post-injection (data not shown). The significant decrease in the PFV in SNP-treated groups indicates an OphA vasodilation, consistent with previous reports on the role of NO in the regulation of basal vascular tone in the OphA and resting CBF.32 The relative decrease of the PFV was more pronounced in females versus males, indicating sex-specific differences of OphA vasoreactivity to NO donors. The parameters extracted from OphA's blood flow velocity waveforms at 3 min post-injection from different groups are shown in Table 1.

In parallel, we monitored the changes in systemic mean BP (MBP) in response to nitroprusside via the non-invasive tail-cuff method. i.p. SNP caused a rapid drop in systemic BP, with a maximal effect 3 min post-injection (Figure 4C). The MBP recovered more quickly compared to the change in the OphA PFV. BP recovered by 50% at 6 min and was fully restored by 11 min after SNP.

# The OphA PFV response to sequential surgical obstruction of common carotid arteries

Transient occlusion of both common carotid arteries is a simple and reliable method to induce transient global cerebral ischemia (tGCI). tGCI is widely used to study ischemic events downstream of the common carotid arteries and ICA, including changes in blood flow in eye diseases. 33,34 To validate the potential of our method for the use in the tGCI model, we recorded real-time changes in left OphA blood flow during sequential mechanical obstruction of the right and left carotid arteries (Figure 5). The right carotid artery closure caused a slight temporary decline within 1 min (Figure 5B, RCc [right carotid closed]), whereas the 3-s closure of the left carotid artery abolished OphA blood flow to the left eye (Figure 5B, LCc [left carotid closed]). Reopening of the left carotid restored OphA flow with an initial hyperemic response and then a gradual decrease to the baseline. Re-opening of the right carotid artery fully restored the initial baseline. Our data clearly demonstrate that our method is suitable to study OphA vascular function in the tGCI mouse model.

### **DISCUSSION**

Dysregulation of ocular blood flow is an important pathological factor contributing to visual impairment.<sup>2,3,35</sup> The OphA plays an essential role in the health of the eye since it supplies blood



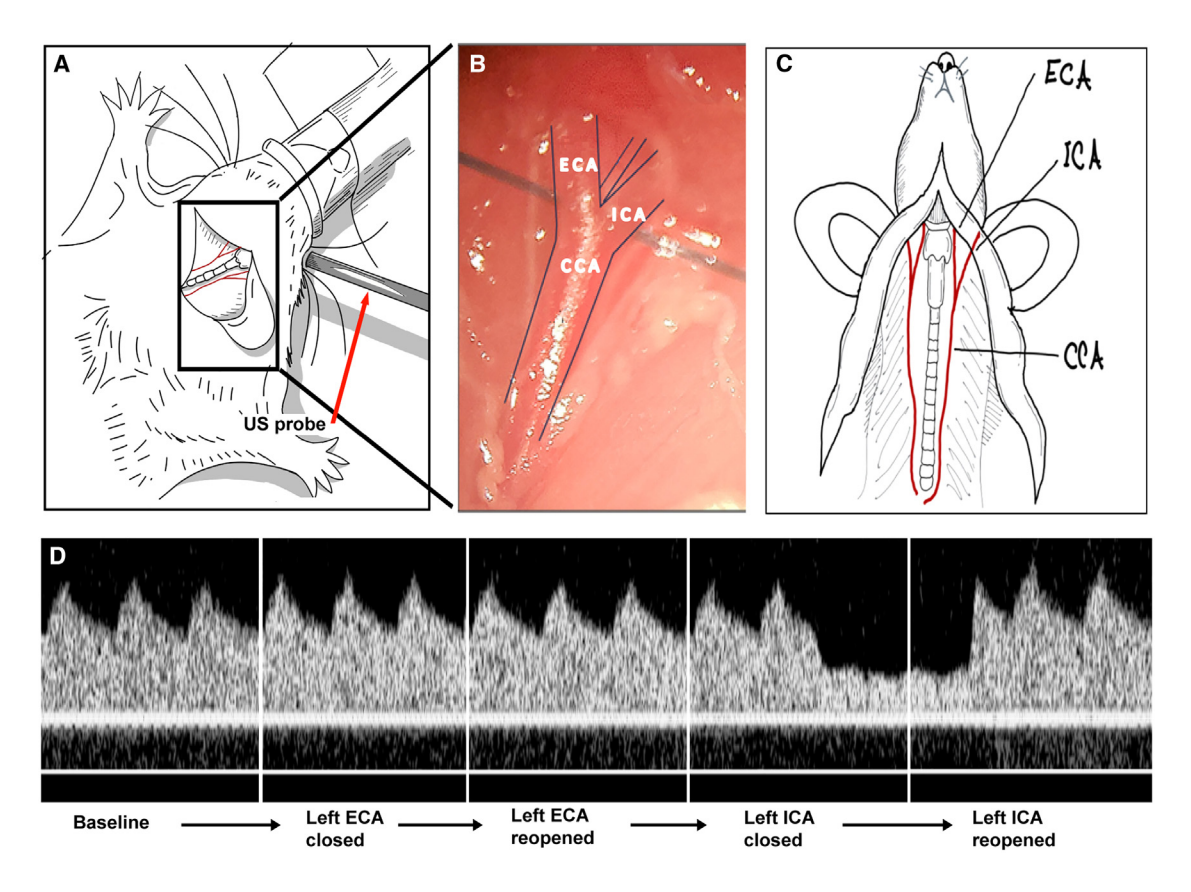


Figure 3. Targeted artery (OphA) originates as a branch off the ICA

(A) Experimental setup for sequential ECA and ICA branch occlusion. A surgically prepared mouse on the heated board with continuous ECG monitoring, the Doppler probe, and the dissected area are shown.

- (B) Magnified view of the neck region prepared for occlusion. CCA, common carotid artery; ICA, internal carotid artery; ECA, external carotid artery.
- (C) Schematic representation of anatomical features in close proximity to CCA and ICA/ECA branching site (adapted from Liu et al. 87).
- (D) Changes of the Doppler signal during sequential occlusion of the blood flow in left ECA and ICA. A representative of 6 independent sequential occlusions from 3 individual mice is shown.

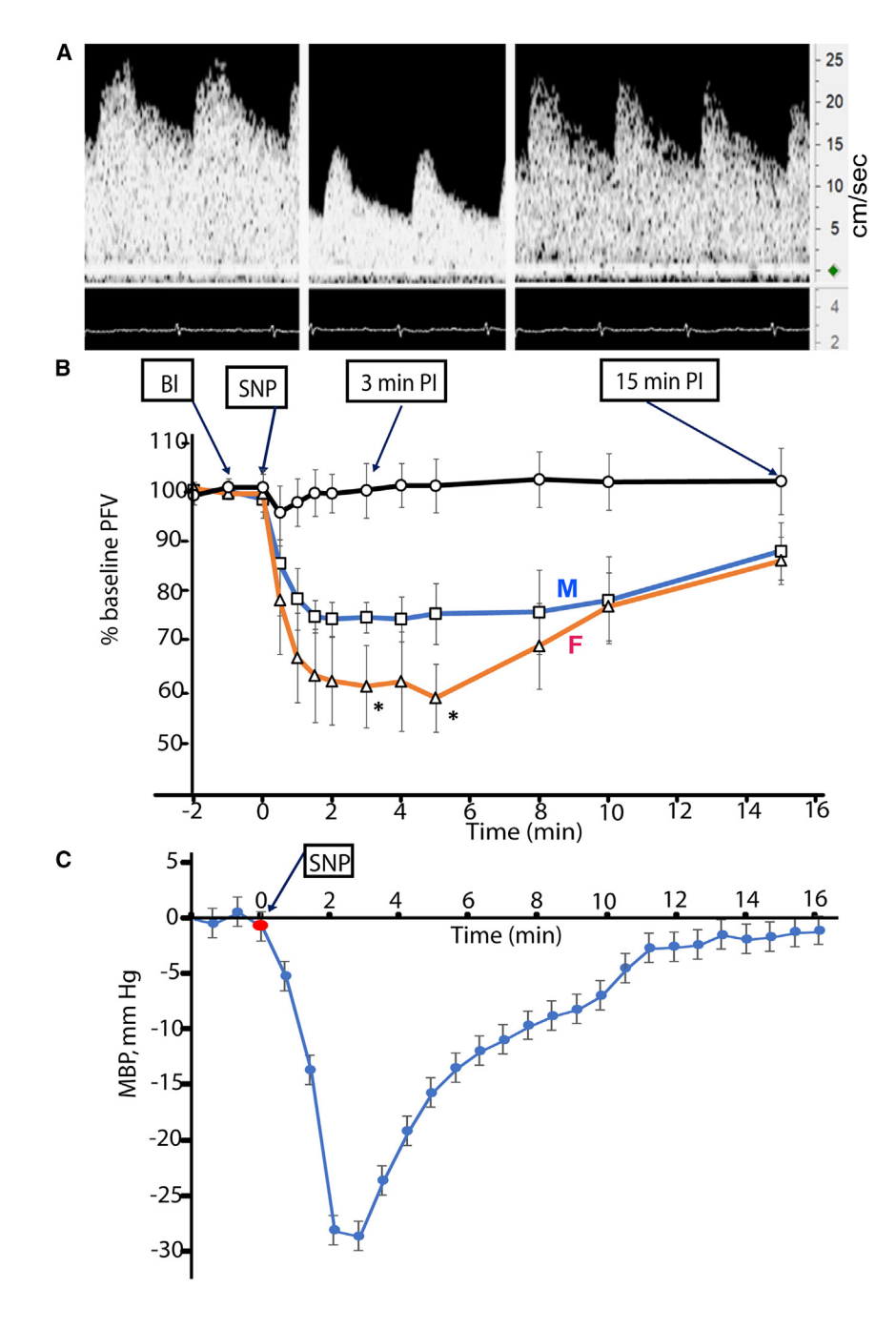
to multiple critical eye structures, including the retina, optic nerve, choroid, and part of the sclera. In addition, the OphA provides essential blood flow to the extraocular muscle, lacrimal gland, eyelid, and conjunctiva. Impaired vasoreactivity and compromised OphA blood flow is closely associated with (or is a critical contributor to) ocular vascular disease and various eye pathologies. <sup>2,3,35</sup>

Mouse models provide critical information relating to the molecular mechanisms of vascular disorders due to their genetic similarity to humans and comparable ocular anatomy and physiology. The repertoire of mouse models of different pathologies and mechanisms of ocular blood flow continues to expand, and the necessity for characterizing new strains is likely to increase in the future. <sup>1,36–38</sup> Determining the dynamic blood flow parameters of the OphA is important to characterize the function of this major cranial blood vessel. Non-invasive *in vivo* characterization of murine blood flow in intracranial blood vessels remains a challenge.

A number of methods have been developed to evaluate ocular and, more specifically, retinal blood flow and vascular reactivity in retinal artery (a major branch of the OphA). Optical techniques, such as camera-based retinal funduscopy, 39 optical coherence tomography angiography (OCTA),40 Doppler OCT, or laser speckle flowgraphy, 41 provide information on changes in retinal blood vessel diameters in response to various stimuli. Laser Doppler velocimetry (LVD) or laser Doppler flowmetry (LDF) can also register changes in retinal blood vessel parameters and determine blood flow. 42 Invasive techniques, such as dyebased angiography, 43 fluorescent labeling of red blood cells, or ex vivo light microscopy on excised eye globe preparations, 42 are also used to evaluate vascular reactivity in the retina. However, most of these techniques are impeded by opacification of the ocular media. The major limitation of these methods is that they measure changes in retinal artery and retinal vasculature, thus only indirectly reflecting the function of the upstream OphA. The current report demonstrates that a high-frequency Doppler ultrasound system can be adopted to directly and non-invasively evaluate the blood flow and vasoreactivity of the OphA in mouse models.

By scanning the surface in the orbital opening with the 20-mHz ultrasound probe, we identified a position near the temporal canthus of the eye that exhibits a rapidly increasing systolic





peak followed by a dicrotic notch and a gradually decreasing diastolic phase, characteristic of arterial blood flow. The 30 cm/s signal amplitude is highly similar to the human eye artery Doppler signal. While the probe location suggested that the OphA was a potential target, definitive confirmation was required. MicroCT imaging and 3D reconstruction of the US trajectory (Figure 2; Video S1) pointed to the position of the OphA as it emerged from the optic canal. *In vivo* microCT imaging with vascular contrast identified the OphA as the single blood vessel of sufficient size, position, and orientation capable of generating the observed ultrasound signal (Figures 2D–2F). Mechanical oc-

# Figure 4. Hemodynamic response to SNP bolus

(A) OphA blood flow velocity (BFV; cm/s) waveforms at baseline (BL), 3 min post-injection (3 min Pl), and 15 min Pl.

(B) Dynamics of OphA PFV changes in anesthetized mice after 1 mg/kg SNP injection, plotted as a percentage of baseline. Data are mean  $\pm$  SD for 3-month-old male (M; n=5), female (F; n=5), and control (C; n=10) mice. Control mice were injected with PBS. \*p<0.05 versus females (twoway ANOVA and Bonferroni multi-comparison test).

(C) Dynamic changes in systemic blood pressure following SNP injection. Data are mean  $\pm$  SD for 3 male and 3 female mice.

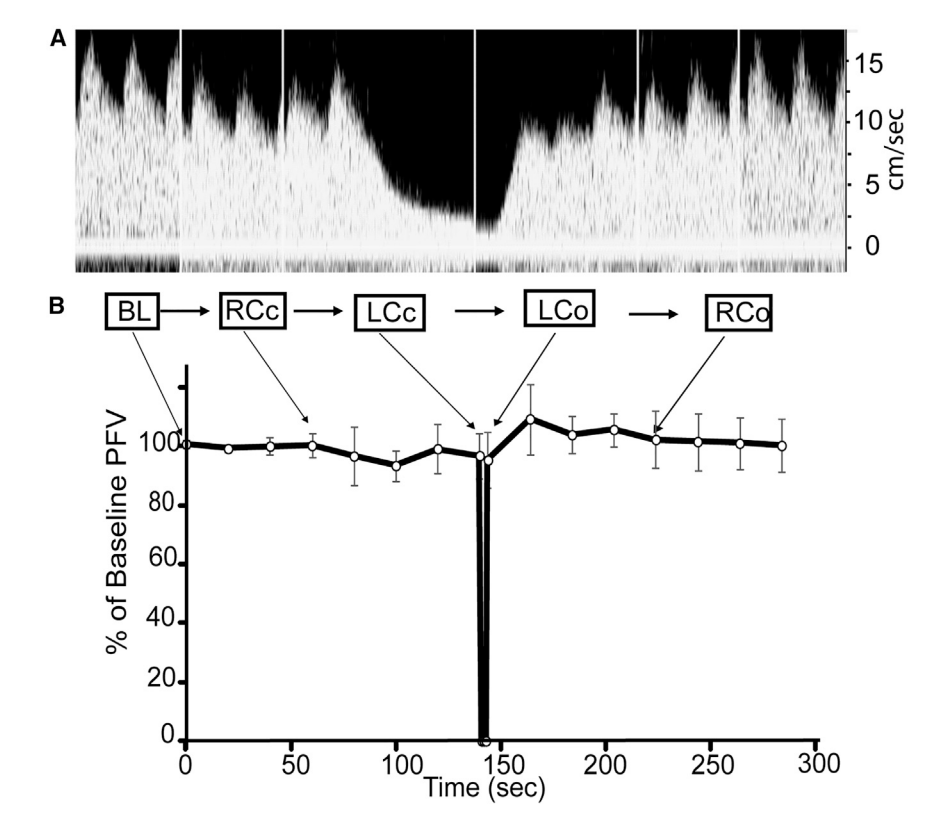
clusion of the ICA branch, but not the ECA branch, of the carotid artery disrupted the acquired Doppler signal (Figure 3), consistent with our imaging-based assignment of the OphA as the signal source.

Despite having a different embryological origin from cerebral arteries,44 the OphA has several important connections and similarities that also make it relevant for assessing cerebral circulation in certain contexts.<sup>45</sup> Similar to the middle cerebral artery (MCA), the OphA branches from the ICA. The OphA has intracranial. intracanalicular, and intraorbital courses. It originates as a branch off the ICA and then passes through the optic canal and into the orbit.44 The OphA is the first branch of the ICA distal to the cavernous sinus and can serve as an important collateral pathway between the ICA and ECA systems. 46,47 Besides its structural similarity, the OphA has functional similarities to cerebral arteries. For instance, the OphA also has myogenic autoregulatory properties,48 which are well documented by classical ex vivo ocular blood flow studies<sup>49</sup> and a number of clinical investigations of the blood flow and vascular tone of retinal circulation. 50,51 The OphA

is involved in similar pathologies as cerebral arteries, such as occlusions, embolic events, and transient ischemic attacks. <sup>52–54</sup> Analogous risk factors for cerebrovascular disease, like hypertension, diabetes, and atherosclerosis, affect the function of the OphA and increase the risk of OphA pathology. <sup>55–57</sup> Vasomotor reactivity was found to be similar in MCA and OphA in cases of severe carotid artery stenosis. <sup>58</sup> Thus, the OphA's ICA origin, its partial intracranial course, the presence of myogenic autoregulation, and similar dysfunction caused by pathologies of the carotid artery suggest that the measurement of OphA blood flow can be used as an accessible surrogate for large cerebral arteries when

Report





investigating some of the pharmacological or surgical interventions affecting cerebrovascular function. In fact, it has been reported that the vasoreactivity of OphA-derived retinal vessels exhibits a diagnostic correlation with cerebral microvascular dysfunction, <sup>59</sup> suggesting that retinal vascular function may serve as a diagnostic surrogate for cerebral vascular function.

One of the emerging concepts in the rapeutic approaches to neurodegeneration is that cerebrovascular function plays a key role in the etiology and progression of cognitive impairment.<sup>60</sup> However, currently, there are very few non-invasive tools available for continuous assessment of CBF in mice. Autoradiography, a gold-standard method for the determination of regional CBF, does not provide temporal information on CBF changes, cannot be used to study longitudinal CBF responses during disease progression or drug treatment, and requires the use of radiolabeled isotopes and animal sacrifice for the analysis. 61 Several in vivo optical techniques based on dynamic light scattering, such as LDF,62 laser speckle contrast imaging,63 and near-infrared diffuse correlation spectroscopy, 64 have emerged to assess CBF at the microvasculature level.<sup>65</sup> Recent additions include molecular dynamic analysis of indocyanine green<sup>66</sup> and in vivo X-ray angiography using synchrotron radiation.<sup>67</sup> A 3D ultrasound system used to image brain vasculature and measure blood flow velocities was described.<sup>68</sup> Implantable optical sensors in mice, circumventing the effects of restraint and anesthesia on hemodynamic parameters, have also been described. 69-71 Functional ultrasound imaging (fUI) has been developed to characterize pharmacologically induced dynamic changes in rodent brain perfusion.<sup>72</sup> This method requires the surgical installation of a metal frame fixed

Figure 5. OphA PVF changes during sequential surgical ligation of common carotid arteries

(A) OphA blood flow velocity waveforms showing changes in PFV at baseline, carotid artery occlusion, and after re-opening of left and right carotid arteries. The sequence: BL (baseline), RCc (right common carotid closed), LCc (left common carotid closed), LCo (left common carotid re-opened), and RCo (right common carotid re-opened).

(B) PFV changes during surgical manipulations presented as a percentage of baseline. Data are mean  $\pm$  SD from 6-month-old BALB/C males (n = 5).

to the animal's skull for the ultrasound probe. The skyll for the ultrasound probe. In summary, most of these methods have limited penetration depth and are invasive, as they require various surgical procedures to create a window for observation. The need for costly state-of-the-art laser systems and restrictions on spatial and temporal resolution limit the use of these technologies by many smaller research groups worldwide.

Non-invasive and longitudinal monitoring of experimentally induced vasoreactivity and change of blood flow at the origin of retinal blood supply, i.e., at

the OphA site, may be even more relevant to cerebrovascular function. The method described in this report offers these opportunities together with higher resolution and low cost. The pulsed Doppler ultrasound-based flow velocity measurement system, originally developed for human vessels, was successfully adapted for use in mice, with their much smaller blood vessel diameters and significantly higher heart rates. 14,19,27 It successfully measured blood flow velocities in ascending, descending, and abdominal aortas and right and left renal, right and left carotid, and celiac arteries of the mouse. 7,8 This report expands the repertoire of the measurements by this Doppler system to the OphA.

Cerebrovascular reactivity and cerebral autoregulation are key mechanisms regulating CBF. The ability of cerebral vessels to constrict and dilate in response to multiple stimuli, including changes in systemic BP, arterial blood gases, cerebral metabolism, or the autonomic nervous system, is essential for maintaining a stable CBF. NO signaling has a vital role in the autochemoregulation of CBF in basal, hypocapnic, and hypercapnic conditions in humans. 74 Arterial pulse pressure regulates endothelial NO synthase in cerebral vessels ex vivo, thereby controlling cerebrovascular reactivity.32 However, precise molecular mechanisms of these critical responses remain largely unknown, in part due to the limiting array of techniques available to study CBF in vivo in animal models. The method described in this report recorded the real-time kinetics of blood flow velocity changes in response to NO-donor nitroprusside in the mouse OphA (Figure 4). OphA vasoreactivity is different from the reactivity of the systemic circulation. As expected from previous



reports, 75,76 i.p. administration of nitroprusside resulted in a rapid drop in systemic BP (Figure 4C) as well as the OphA blood flow velocity (Figure 4A). However, the recovery dynamics of the OphA and systemic circulation (Figures 4B and 4C) are significantly different. Systemic BP was essentially restored 11 min post-nitroprusside, while the OphA blood flow velocity was only partially recovered even 16 min later. These different hemodynamic responses clearly demonstrate that OphA blood flow regulation is independent of that of the systemic circulation. The sensitivity of the described method revealed that vasoreactivity to NO donors of the mouse OphA is sex specific (Figure 4B). Conversely, we observed no sex differences in the systemic BP response to nitroprusside, similar to previous reports on wildtype mice. 76,77 The approach described here may be useful for unraveling the impact of sex hormones on ophthalmic circulation or facilitating the screening of sex-specific therapeutics.

Up to 80% of human strokes are ischemic, resulting from cerebral artery occlusion.<sup>78</sup> Presently, there is no effective treatment or prevention for brain ischemia. The obstructed blood flow and reduced brain perfusion causes neuronal death and increases the risk of stroke and neurodegeneration, including various dementias.<sup>79</sup> The molecular mechanisms involved in neurodegeneration and retinal damage caused by tGCl due to decreased blood flow are the subject of intense investigations.<sup>80–83</sup> The transient occlusion of both common carotid arteries by sutures (two-vessel occlusion [2VO]<sup>34</sup>) is a common model used to investigate the development of neurodegeneration and retinal dysfunction after occlusion.<sup>80,82,84</sup>

We demonstrated that our approach can be applied to monitor in real time and with high precision and temporal resolution the fast kinetics of OphA blood flow responses in the 2VO tGCI model (Figure 5). Our results show that the OphA closely mimics the behavior of CBF in conditions of carotid artery occlusion. The non-invasive nature of our approach allows previously inaccessible longitudinal assessment of pre-ischemic, during, and post-ischemic vascular OphA responses in the same animal. The baseline flow assessment and normalization in the same mouse significantly reduce parameter variations in each individual animal (Table 1). The real-time imaging in our approach can be used as feedback to guide and follow surgical manipulations to achieve a desirable level of occlusion. The use of our approach to the tGCI model in transgenic mice strains could provide new insights into the molecular mechanisms of ischemia/reperfusion injury and facilitate the discovery of new neuroprotective agents.

### **Limitations of the study**

The application of the Doppler principle to determine blood flow velocity imposes specific limitations on the method, which should be considered during data collection and evaluation.

The first factor to consider is the lack of imaging for guidance for placing the ultrasound probe.

The specific location of the mouse anatomy described here, the shape of arterial velocity wave form, and the timing of the signal with respect to the electrocardiogram (ECG) help to overcome this limitation.

The second factor is the alignment of the Doppler transducer to parallel the sound beam to the axis of the vessel and the normal direction of flow. The optimal Doppler angle is  $\sim$ 0°, which

is reflected in the maximal amplitude of the velocity waveform.<sup>29</sup> The spectral peak or maximum velocity waveform is the most robust parameter in the Doppler signal, though other parameters can be reliably extracted by DFVS software (Table 1). The small footprint of the used Doppler probe (2.25 mm) allows for the optimal alignment (usually <30°) of the sound beam to the direction of the blood flow. This ensures that the percentage of errors in the peak velocity measurement is low when the angle of measurement is within 5° of the true angles. 14,85 The manual adjustment of the probe position guided by the visual image of the signal waveform, amplitude of the signal, and supporting audio signal allows for high reproducibility with absolute numbers for major recorded parameters to be reached (Table 1) and proper probe placement achieved in under 10 min. Achieving the appropriate shape (a low-resistance flow waveform<sup>64</sup>) and optimal amplitude (Figure S1) of the signal is critical for the quality and reproducibility of the experimental data.

The third factor to consider is that Doppler measurements are susceptible to motion artifacts. For consistent, uninterrupted recording, animal anesthesia is necessary. The application of minimally effective levels of isoflurane anesthesia <sup>86</sup> helps to preserve the vasodilative properties of the OphA. The use of a lockable micro-manipulator for the duration of the experiment also stabilizes the position of the probe. The use of a stereotactic head device could offer further improvements.

Despite the inherent limitations outlined above, the variability of absolute PFV values in our experiments did not exceed 15%, which allowed us to achieve statistical significance for most experimental groups (Table 1). Expressing changes of the PVF as a percentage of baseline for each individual experimental animal further minimized the variability and improved statistical significance between groups (Table 1).

The advantages and disadvantages of the DFVS system used in our studies are described in greater detail elsewhere. 19,27

### **RESOURCE AVAILABILITY**

### Lead contact

Requests for protocols and reagents can be directed to lead contact, Iraida Sharina (iraida.g.sharina@uth.tmc.edu).

### **Materials availability**

No unique reagents or equipment were generated in this study. All equipment and materials were resourced from commercial vendors. Details about the materials or instruments can be provided upon request by the lead contact, Iraida Sharina (iraida.g.sharina@uth.tmc.edu).

### Data and code availability

- No original code was generated in this study.
- All data generated in this study are available within the article or upon request from the lead contact, Iraida Sharina (iraida.g.sharina@uth. tmc.edu).
- Any additional information needed to reanalyze the data reported in this
  paper is available from the lead contact by request.

### **ACKNOWLEDGMENTS**

The authors are grateful to Mr. Muhammad Awad for the assistance with generating figures' cartoon graphics. This study was supported by grants from the National Institutes of Health (NIH; RAG071999A to I.S., HL139838 to E.M., and R01 AG081942 and R56 AG084130 to S.P.M.) and the American

### Report



Heart Association (23TPA1070711 to E.M.). MicroCT imaging was supported by NIH S10OD030336 (S.P.M.) and performed through the MicroCT Imaging Facility at the McGovern Medical School at UTHealth.

#### **AUTHOR CONTRIBUTIONS**

I.S., S.P.M., and A.K.R. conceptualized the research project. I.S. supervised the research project. A.K.R., S.P.M., R.A., S.C., and E.M. participated in method validation and performance of the experiments. R.A. and S.C. analyzed the collected data and produced the graphics for the presented figures. I.S., S.P.M., R.A., S.C., E.M., and A.K.R. participated in writing the original draft of the manuscript. I.S., S.P.M., and A.K.R. were responsible for reviewing and final editing of the paper.

#### **DECLARATION OF INTERESTS**

A.K.R. is working full-time as a principal scientist at Indus Instruments and is an adjunct assistant professor in the Section of Cardiovascular Research, Department of Medicine at Baylor College of Medicine, Houston, Texas.

#### **STAR**\*METHODS

Detailed methods are provided in the online version of this paper and include the following:

- KEY RESOURCES TABLE
- EXPERIMENTAL MODEL AND STUDY PARTICIPANT DETAILS
- METHOD DETAILS
  - Doppler signal detection in OphA using DFVS
  - Ophthalmic artery identification
- QUANTIFICATION AND STATISTICAL ANALYSIS

### SUPPLEMENTAL INFORMATION

Supplemental information can be found online at https://doi.org/10.1016/j.crmeth.2025.100983.

Received: August 3, 2023 Revised: September 25, 2024 Accepted: January 24, 2025 Published: February 14, 2025

### **REFERENCES**

- Hanaguri, J., Yokota, H., Watanabe, M., Yamagami, S., Kushiyama, A., Kuo, L., and Nagaoka, T. (2021). Retinal blood flow dysregulation precedes neural retinal dysfunction in type 2 diabetic mice. Sci. Rep. 11, 18401. https://doi.org/10.1038/s41598-021-97651-3.
- Moore, D., Harris, A., Wudunn, D., Kheradiya, N., and Siesky, B. (2008).
   Dysfunctional regulation of ocular blood flow: A risk factor for glaucoma?
   Clin. Ophthalmol. 2, 849–861. https://doi.org/10.2147/opth.s2774.
- Toda, N., and Nakanishi-Toda, M. (2007). Nitric oxide: ocular blood flow, glaucoma, and diabetic retinopathy. Prog. Retin. Eye Res. 26, 205–238. https://doi.org/10.1016/j.preteyeres.2007.01.004.
- Dawson, T.M., Golde, T.E., and Lagier-Tourenne, C. (2018). Animal models of neurodegenerative diseases. Nat. Neurosci. 21, 1370–1379. https://doi.org/10.1038/s41593-018-0236-8.
- Shah, S.S., and Khanam, S. (2024). Orbital Color Doppler Imaging (Stat-Pearls).
- Fantini, S., Sassaroli, A., Tgavalekos, K.T., and Kornbluth, J. (2016). Cerebral blood flow and autoregulation: current measurement techniques and prospects for noninvasive optical methods. Neurophotonics 3, 031411. https://doi.org/10.1117/1.NPh.3.3.031411.
- Hartley, C.J., Reddy, A.K., Madala, S., Entman, M.L., Michael, L.H., and Taffet, G.E. (2011). Doppler velocity measurements from large and small

- arteries of mice. Am. J. Physiol. Heart Circ. Physiol. 301, H269–H278. https://doi.org/10.1152/ajpheart.00320.2011.
- Hartley, C.J., Taffet, G.E., Reddy, A.K., Entman, M.L., and Michael, L.H. (2002). Noninvasive cardiovascular phenotyping in mice. ILAR J. 43, 147–158. https://doi.org/10.1093/ilar.43.3.147.
- Wikstrom, J., Gronros, J., Bergstrom, G., and Gan, L.M. (2005). Functional and morphologic imaging of coronary atherosclerosis in living mice using high-resolution color Doppler echocardiography and ultrasound biomicroscopy. J. Am. Coll. Cardiol. 46, 720–727. https://doi.org/10.1016/j. jacc.2005.04.053.
- Williams, R., Needles, A., Cherin, E., Zhou, Y.Q., Henkelman, R.M., Adamson, S.L., and Foster, F.S. (2007). Noninvasive ultrasonic measurement of regional and local pulse-wave velocity in mice. Ultrasound Med. Biol. 33, 1368–1375. https://doi.org/10.1016/j.ultrasmedbio.2007.03.012.
- Mace, E., Montaldo, G., Cohen, I., Baulac, M., Fink, M., and Tanter, M. (2011). Functional ultrasound imaging of the brain. Nat. Methods 8, 662–664. https://doi.org/10.1038/nmeth.1641.
- Mace, E., Montaldo, G., Osmanski, B.F., Cohen, I., Fink, M., and Tanter, M. (2013). Functional ultrasound imaging of the brain: theory and basic principles. IEEE Trans. Ultrason. Ferroelectrics Freq. Control 60, 492–506. https://doi.org/10.1109/TUFFC.2013.2592.
- Macgowan, C.K., Stoops, S.J., Zhou, Y.Q., Cahill, L.S., and Sled, J.G. (2015). Evaluation of cerebrovascular impedance and wave reflection in mouse by ultrasound. J. Cerebr. Blood Flow Metabol. 35, 521–526. https://doi.org/10.1038/jcbfm.2014.229.
- Reddy, A.K., Madala, S., Jones, A.D., Caro, W.A., Eberth, J.F., Pham, T.T., Taffet, G.E., and Hartley, C.J. (2009). Multichannel pulsed Doppler signal processing for vascular measurements in mice. Ultrasound Med. Biol. 35, 2042–2054. https://doi.org/10.1016/j.ultrasmedbio.2009.06.1096.
- Purkayastha, S., and Sorond, F. (2012). Transcranial Doppler ultrasound: technique and application. Semin. Neurol. 32, 411–420. https://doi.org/ 10.1055/s-0032-1331812.
- Schatlo, B., Gläsker, S., Zauner, A., Thompson, B.G., Oldfield, E.H., and Pluta, R.M. (2009). Continuous neuromonitoring using transcranial Doppler reflects blood flow during carbon dioxide challenge in primates with global cerebral ischemia. Neurosurgery 64, 1148–1154. https://doi. org/10.1227/01.NEU.0000343542.61238.DF.
- D'Andrea, A., Conte, M., Scarafile, R., Riegler, L., Cocchia, R., Pezzullo, E., Cavallaro, M., Carbone, A., Natale, F., Russo, M.G., et al. (2016). Transcranial Doppler Ultrasound: Physical Principles and Principal Applications in Neurocritical Care Unit. J. Cardiovasc. Echogr. 26, 28–41. https://doi.org/ 10.4103/2211-4122.183746.
- Hartley, C.J., and Cole, J.S. (1974). An ultrasonic pulsed Doppler system for measuring blood flow in small vessels. J. Appl. Physiol. 37, 626–629. https://doi.org/10.1152/jappl.1974.37.4.626.
- Reddy, A.K., Jones, A.D., Martono, C., Caro, W.A., Madala, S., and Hartley, C.J. (2005). Pulsed Doppler signal processing for use in mice: design and evaluation. IEEE Trans. Biomed. Eng. 52, 1764–1770. https://doi.org/10.1109/tbme.2005.855710.
- 20. Borowy, C.S., and Mukhdomi, T. (2024). Sonography Physical Principles and Instrumentation (StatPearls).
- Gerstenmayer, M., Fellah, B., Magnin, R., Selingue, E., and Larrat, B. (2018). Acoustic Transmission Factor through the Rat Skull as a Function of Body Mass, Frequency and Position. Ultrasound Med. Biol. 44, 2336–2344. https://doi.org/10.1016/j.ultrasmedbio.2018.06.005.
- Cramer, S.W., Carter, R.E., Aronson, J.D., Kodandaramaiah, S.B., Ebner, T.J., and Chen, C.C. (2021). Through the looking glass: A review of cranial window technology for optical access to the brain. J. Neurosci. Methods 354, 109100. https://doi.org/10.1016/j.jneumeth.2021.109100.
- Yang, G., Pan, F., Parkhurst, C.N., Grutzendler, J., and Gan, W.B. (2010). Thinned-skull cranial window technique for long-term imaging of the cortex in live mice. Nat. Protoc. 5, 201–208. https://doi.org/10.1038/nprot. 2009.222.



- Plog, B.A., Lou, N., Pierre, C.A., Cove, A., Kenney, H.M., Hitomi, E., Kang, H., Iliff, J.J., Zeppenfeld, D.M., Nedergaard, M., and Vates, G.E. (2020). When the air hits your brain: decreased arterial pulsatility after craniectomy leading to impaired glymphatic flow. J. Neurosurg. 133, 210–223. https://doi.org/10.3171/2019.2.JNS182675.
- Holtmaat, A., Bonhoeffer, T., Chow, D.K., Chuckowree, J., De Paola, V., Hofer, S.B., Hübener, M., Keck, T., Knott, G., Lee, W.C.A., et al. (2009). Long-term, high-resolution imaging in the mouse neocortex through a chronic cranial window. Nat. Protoc. 4, 1128–1144. https://doi.org/10. 1038/nprot.2009.89.
- Wang, X., Luo, Y., Chen, Y., Chen, C., Yin, L., Yu, T., He, W., and Ma, C. (2021). A Skull-Removed Chronic Cranial Window for Ultrasound and Photoacoustic Imaging of the Rodent Brain. Front. Neurosci. 15, 673740. https://doi.org/10.3389/fnins.2021.673740.
- Reddy, A.K., Taffet, G.E., Li, Y.H., Lim, S.W., Pham, T.T., Pocius, J.S., Entman, M.L., Michael, L.H., and Hartley, C.J. (2005). Pulsed Doppler signal processing for use in mice: applications. IEEE Trans. Biomed. Eng. 52, 1771–1783. https://doi.org/10.1109/TBME.2005.855709.
- Li, Y.H., Reddy, A.K., Taffet, G.E., Michael, L.H., Entman, M.L., and Hartley, C.J. (2003). Doppler evaluation of peripheral vascular adaptations to transverse aortic banding in mice. Ultrasound Med. Biol. 29, 1281–1289. https://doi.org/10.1016/s0301-5629(03)00986-4.
- Meola, M., Ibeas, J., Lasalle, G., and Petrucci, I. (2021). Basics for performing a high-quality color Doppler sonography of the vascular access.
   J. Vasc. Access 22, 18–31. https://doi.org/10.1177/11297298211018060.
- Laspas, P., Goloborodko, E., Sniatecki, J.J., Kordasz, M.L., Manicam, C., Wojnowski, L., Li, H., Patzak, A., Pfeiffer, N., and Gericke, A. (2014). Role of nitric oxide synthase isoforms for ophthalmic artery reactivity in mice. Exp. Eye Res. 127, 1–8. https://doi.org/10.1016/j.exer.2014.06.018.
- Manicam, C., Staubitz, J., Brochhausen, C., Grus, F.H., Pfeiffer, N., and Gericke, A. (2016). The Gatekeepers in the Mouse Ophthalmic Artery: Endothelium-Dependent Mechanisms of Cholinergic Vasodilation. Sci. Rep. 6, 20322. https://doi.org/10.1038/srep20322.
- Raignault, A., Bolduc, V., Lesage, F., and Thorin, E. (2017). Pulse pressuredependent cerebrovascular eNOS regulation in mice. J. Cerebr. Blood Flow Metabol. 37, 413–424. https://doi.org/10.1177/0271678X16629155.
- Augustin, H.G., and Koh, G.Y. (2017). Organotypic vasculature: From descriptive heterogeneity to functional pathophysiology. Science 357, eaal2379. https://doi.org/10.1126/science.aal2379.
- Leon-Moreno, L.C., Castaneda-Arellano, R., Rivas-Carrillo, J.D., and Duenas-Jimenez, S.H. (2020). Challenges and Improvements of Developing an Ischemia Mouse Model Through Bilateral Common Carotid Artery Occlusion. J. Stroke Cerebrovasc. Dis. 29, 104773. https://doi.org/10.1016/j.jstrokecerebrovasdis.2020.104773.
- Luo, X., Shen, Y.M., Jiang, M.N., Lou, X.F., and Shen, Y. (2015). Ocular Blood Flow Autoregulation Mechanisms and Methods. J. Ophthalmol. 2015, 864871. https://doi.org/10.1155/2015/864871.
- McDowell, C.M., Kizhatil, K., Elliott, M.H., Overby, D.R., van Batenburg-Sherwood, J., Millar, J.C., Kuehn, M.H., Zode, G., Acott, T.S., Anderson, M.G., et al. (2022). Consensus Recommendation for Mouse Models of Ocular Hypertension to Study Aqueous Humor Outflow and Its Mechanisms. Invest. Ophthalmol. Vis. Sci. 63, 12. https://doi.org/10.1167/jovs.63.2.12
- Mukai, R., Park, D.H., Okunuki, Y., Hasegawa, E., Klokman, G., Kim, C.B., Krishnan, A., Gregory-Ksander, M., Husain, D., Miller, J.W., and Connor, K.M. (2019). Mouse model of ocular hypertension with retinal ganglion cell degeneration. PLoS One 14, e0208713. https://doi.org/10.1371/journal.pone.0208713.
- Pang, I.H., and Clark, A.F. (2020). Inducible rodent models of glaucoma. Prog. Retin. Eye Res. 75, 100799. https://doi.org/10.1016/j.preteyeres. 2019.100799.
- DeBuc, D.C., Rege, A., and Smiddy, W.E. (2021). Use of XyCAM RI for Noninvasive Visualization and Analysis of Retinal Blood Flow Dynamics

- During Clinical Investigations. Expet Rev. Med. Dev. 18, 225–237. https://doi.org/10.1080/17434440.2021.1892486.
- Spaide, R.F., Fujimoto, J.G., Waheed, N.K., Sadda, S.R., and Staurenghi, G. (2018). Optical coherence tomography angiography. Prog. Retin. Eye Res. 64, 1–55. https://doi.org/10.1016/j.preteyeres.2017.11.003.
- Wei, X., Balne, P.K., Meissner, K.E., Barathi, V.A., Schmetterer, L., and Agrawal, R. (2018). Assessment of flow dynamics in retinal and choroidal microcirculation. Surv. Ophthalmol. 63, 646–664. https://doi.org/10.1016/ j.survophthal.2018.03.003.
- Bohm, E.W., Pfeiffer, N., Wagner, F.M., and Gericke, A. (2022). Methods to measure blood flow and vascular reactivity in the retina. Front. Med. 9, 1069449. https://doi.org/10.3389/fmed.2022.1069449.
- Schmetterer, L., and Garhofer, G. (2007). How can blood flow be measured? Surv. Ophthalmol. 52, S134–S138. https://doi.org/10.1016/j. survophthal.2007.08.008.
- Toma, N. (2016). Anatomy of the Ophthalmic Artery: Embryological Consideration. Neurol. Med.-Chir. 56, 585–591. https://doi.org/10.2176/ nmc.ra.2015-0324.
- Singh, R.B., Saini, C., Shergill, S., and Agarwal, A. (2020). Window to the circulatory system: Ocular manifestations of cardiovascular diseases. Eur. J. Ophthalmol. 30, 1207–1219. https://doi.org/10.1177/ 1120672120914232.
- Jung, S., Wiest, R., Gralla, J., McKinley, R., Mattle, H., and Liebeskind, D. (2017). Relevance of the cerebral collateral circulation in ischaemic stroke: time is brain, but collaterals set the pace. Swiss Med. Wkly. 147, w14538. https://doi.org/10.4414/smw.2017.14538.
- Michalinos, A., Zogana, S., Kotsiomitis, E., Mazarakis, A., and Troupis, T. (2015). Anatomy of the Ophthalmic Artery: A Review concerning Its Modern Surgical and Clinical Applications. Anat. Res. Int. 2015, 591961. https://doi.org/10.1155/2015/591961.
- Jarajapu, Y.P.R., Grant, M.B., and Knot, H.J. (2004). Myogenic tone and reactivity of the rat ophthalmic artery. Invest. Ophthalmol. Vis. Sci. 45, 253–259. https://doi.org/10.1167/iovs.03-0546.
- Best, M., Gerstein, D., Wlad, N., Rabinovitz, A.Z., and Hiller, G.H. (1973).
   Autoregulation of ocular blood flow. Arch. Ophthalmol. 89, 143–148.
   https://doi.org/10.1001/archopht.1973.01000040145019.
- Nemeth, J., Knezy, K., Tapaszto, B., Kovacs, R., and Harkanyi, Z. (2002).
   Different autoregulation response to dynamic exercise in ophthalmic and central retinal arteries: a color Doppler study in healthy subjects. Graefes Arch. Clin. Exp. Ophthalmol. 240, 835–840. https://doi.org/10.1007/s00417-002-0552-1.
- Sorrentino, F.S., Matteini, S., Bonifazzi, C., Sebastiani, A., and Parmeggiani, F. (2018). Diabetic retinopathy and endothelin system: microangiopathy versus endothelial dysfunction. Eye 32, 1157–1163. https://doi.org/10.1038/s41433-018-0032-4
- Chen, C., Singh, G., Madike, R., and Cugati, S. (2024). Central retinal artery occlusion: a stroke of the eye. Eye 38, 2319–2326. https://doi.org/10. 1038/s41433-024-03029-w.
- Daruich, A., Robert, M.P., Zola, M., Matet, A., and Bremond-Gignac, D. (2023). Retinal stroke: research models, targets and experimental drugs. Expet Opin. Invest. Drugs 32, 755–760. https://doi.org/10.1080/13543784.2023.2254688.
- Mizener, J.B., Podhajsky, P., and Hayreh, S.S. (1997). Ocular ischemic syndrome. Ophthalmology 104, 859–864. https://doi.org/10.1016/ s0161-6420(97)30221-8.
- Agca, F.V., Sensoy, B., Aslanci, M.E., Ulutas, H.G., and Gunes, A. (2023).
   Retinal microvascular changes in patients with coronary artery disease and apnea. Microvasc. Res. 148, 104514. https://doi.org/10.1016/j.mvr. 2023.104514.
- Meyer, M.L., Klein, B.E., Klein, R., Palta, P., Sharrett, A.R., Heiss, G., Nambi, V., Wong, T.Y., and Tanaka, H. (2020). Central arterial stiffness and retinal vessel calibers: the Atherosclerosis Risk in Communities

### Report



- Study-Neurocognitive Study. J. Hypertens. 38, 266–273. https://doi.org/10.1097/HJH.000000000002252.
- Nguyen, T.T., and Wong, T.Y. (2009). Retinal vascular changes and diabetic retinopathy. Curr. Diabetes Rep. 9, 277–283. https://doi.org/10.1007/s11892-009-0043-4.
- Bornstein, N.M., Gur, A.Y., Geyer, O., and Almog, Y. (2000). Vasomotor reactivity in the ophthalmic artery: different from or similar to intracerebral vessels? Eur. J. Ultrasound 11, 1–6. https://doi.org/10.1016/s0929-8266(99)00065-8.
- Angermann, S., Günthner, R., Hanssen, H., Lorenz, G., Braunisch, M.C., Steubl, D., Matschkal, J., Kemmner, S., Hausinger, R., Block, Z., et al. (2022). Cognitive impairment and microvascular function in end-stage renal disease. Int. J. Methods Psychiatr. Res. 31, e1909. https://doi.org/ 10.1002/mpr.1909.
- Kisler, K., Nelson, A.R., Montagne, A., and Zlokovic, B.V. (2017). Cerebral blood flow regulation and neurovascular dysfunction in Alzheimer disease. Nat. Rev. Neurosci. 18, 419–434. https://doi.org/10.1038/nrn.2017.48.
- Sakurada, O., Kennedy, C., Jehle, J., Brown, J.D., Carbin, G.L., and Sokoloff, L. (1978). Measurement of local cerebral blood flow with iodo [14C] antipyrine. Am. J. Physiol. 234, H59–H66. https://doi.org/10.1152/ajpheart.1978.234.1.H59.
- Ansari, S., Azari, H., McConnell, D.J., Afzal, A., and Mocco, J. (2011). Intraluminal middle cerebral artery occlusion (MCAO) model for ischemic stroke with laser doppler flowmetry guidance in mice. J. Vis. Exp. https://doi.org/10.3791/2879.
- Boas, D.A., and Dunn, A.K. (2010). Laser speckle contrast imaging in biomedical optics. J. Biomed. Opt. 15, 011109. https://doi.org/10.1117/ 1.3285504.
- Cheng, R., Shang, Y., Hayes, D., Jr., Saha, S.P., and Yu, G. (2012). Noninvasive optical evaluation of spontaneous low frequency oscillations in cerebral hemodynamics. Neuroimage 62, 1445–1454. https://doi.org/10.1016/j.neuroimage.2012.05.069.
- Devor, A., Sakadžić, S., Srinivasan, V.J., Yaseen, M.A., Nizar, K., Saisan, P.A., Tian, P., Dale, A.M., Vinogradov, S.A., Franceschini, M.A., and Boas, D.A. (2012). Frontiers in optical imaging of cerebral blood flow and metabolism. J. Cerebr. Blood Flow Metabol. 32, 1259–1276. https://doi.org/10. 1038/jcbfm.2011.195.
- Ku, T., and Choi, C. (2012). Noninvasive optical measurement of cerebral blood flow in mice using molecular dynamics analysis of indocyanine green. PLoS One 7, e48383. https://doi.org/10.1371/journal.pone. 0048383.
- Kidoguchi, K., Tamaki, M., Mizobe, T., Koyama, J., Kondoh, T., Kohmura, E., Sakurai, T., Yokono, K., and Umetani, K. (2006). In vivo X-ray angiography in the mouse brain using synchrotron radiation. Stroke 37, 1856–1861. https://doi.org/10.1161/01.STR.0000226904. 96059 a6
- Demeulenaere, O., Bertolo, A., Pezet, S., Ialy-Radio, N., Osmanski, B., Papadacci, C., Tanter, M., Deffieux, T., and Pernot, M. (2022). In vivo whole brain microvascular imaging in mice using transcranial 3D Ultrasound Localization Microscopy. EBioMedicine 79, 103995. https://doi.org/10.1016/j.ebiom.2022.103995.
- Huang, C., Gu, Y., Chen, J., Bahrani, A.A., Abu Jawdeh, E.G., Bada, H.S., Saatman, K., Yu, G., and Chen, L. (2019). A Wearable Fiberless Optical Sensor for Continuous Monitoring of Cerebral Blood Flow in Mice. IEEE J. Sel. Top. Quant. Electron. 25, 6900108. https://doi.org/10.1109/ JSTQE.2018.2854597.
- Li, Y., Rakymzhan, A., Tang, P., and Wang, R.K. (2020). Procedure and protocols for optical imaging of cerebral blood flow and hemodynamics in awake mice. Biomed. Opt Express 11, 3288–3300. https://doi.org/10. 1364/BOE.394649.
- Yousef Yengej, D.N., Ferando, I., Kechechyan, G., Nwaobi, S.E., Raman, S., Charles, A., and Faas, G.C. (2021). Continuous long-term recording and triggering of brain neurovascular activity and behaviour in freely mov-

- ing rodents. J. Physiol. 599, 4545–4559. https://doi.org/10.1113/ JP281514.
- Hingot, V., Brodin, C., Lebrun, F., Heiles, B., Chagnot, A., Yetim, M., Gauberti, M., Orset, C., Tanter, M., Couture, O., et al. (2020). Early Ultrafast Ultrasound Imaging of Cerebral Perfusion correlates with Ischemic Stroke outcomes and responses to treatment in Mice. Theranostics 10, 7480–7491. https://doi.org/10.7150/thno.44233.
- Rabut, C., Ferrier, J., Bertolo, A., Osmanski, B., Mousset, X., Pezet, S., Deffieux, T., Lenkei, Z., and Tanter, M. (2020). Pharmaco-fUS: Quantification of pharmacologically-induced dynamic changes in brain perfusion and connectivity by functional ultrasound imaging in awake mice. Neuroimage 222, 117231. https://doi.org/10.1016/j.neuroimage.2020. 117231.
- Garry, P.S., Ezra, M., Rowland, M.J., Westbrook, J., and Pattinson, K.T.S. (2015). The role of the nitric oxide pathway in brain injury and its treatment-from bench to bedside. Exp. Neurol. 263, 235–243. https://doi.org/10.1016/j.expneurol.2014.10.017.
- Buys, E.S., Ko, Y.C., Alt, C., Hayton, S.R., Jones, A., Tainsh, L.T., Ren, R., Giani, A., Clerté, M., Abernathy, E., et al. (2013). Soluble guanylate cyclase alpha1-deficient mice: a novel murine model for primary open angle glaucoma. PLoS One 8, e60156. https://doi.org/10.1371/journal.pone. 0060156.
- Buys, E.S., Sips, P., Vermeersch, P., Raher, M.J., Rogge, E., Ichinose, F., Dewerchin, M., Bloch, K.D., Janssens, S., and Brouckaert, P. (2008). Gender-specific hypertension and responsiveness to nitric oxide in sGCalpha1 knockout mice. Cardiovasc. Res. 79, 179–186. https://doi.org/10. 1093/cvr/cvn068.
- Blumer, J.B., Lord, K., Saunders, T.L., Pacchioni, A., Black, C., Lazartigues, E., Varner, K.J., Gettys, T.W., and Lanier, S.M. (2008). Activator of G protein signaling 3 null mice: I. Unexpected alterations in metabolic and cardiovascular function. Endocrinology 149, 3842–3849. https://doi.org/10.1210/en.2008-0050.
- Durukan, A., and Tatlisumak, T. (2007). Acute ischemic stroke: overview of major experimental rodent models, pathophysiology, and therapy of focal cerebral ischemia. Pharmacol. Biochem. Behav. 87, 179–197. https://doi. org/10.1016/j.pbb.2007.04.015.
- Balestrini, S., Perozzi, C., Altamura, C., Vernieri, F., Luzzi, S., Bartolini, M., Provinciali, L., and Silvestrini, M. (2013). Severe carotid stenosis and impaired cerebral hemodynamics can influence cognitive deterioration. Neurology 80, 2145–2150. https://doi.org/10.1212/WNL.0b013e318295d71a.
- Schiavon, A.P., Soares, L.M., Bonato, J.M., Milani, H., Guimarães, F.S., and Weffort de Oliveira, R.M. (2014). Protective effects of cannabidiol against hippocampal cell death and cognitive impairment induced by bilateral common carotid artery occlusion in mice. Neurotox. Res. 26, 307–316. https://doi.org/10.1007/s12640-014-9457-0.
- Soares, L.M., Schiavon, A.P., Milani, H., and de Oliveira, R.M.W. (2013).
   Cognitive impairment and persistent anxiety-related responses following bilateral common carotid artery occlusion in mice. Behav. Brain Res. 249, 28–37. https://doi.org/10.1016/j.bbr.2013.04.010.
- Tsai, S.H., Xie, W., Zhao, M., Rosa, R.H., Jr., Hein, T.W., and Kuo, L. (2018). Alterations of Ocular Hemodynamics Impair Ophthalmic Vascular and Neuroretinal Function. Am. J. Pathol. 188, 818–827. https://doi.org/10.1016/j.ajpath.2017.11.015.
- Zhao, Y., Yu, B., Xiang, Y.H., Han, X.J., Xu, Y., So, K.F., Xu, A.D., and Ruan, Y.W. (2013). Changes in retinal morphology, electroretinogram and visual behavior after transient global ischemia in adult rats. PLoS One 8, e65555. https://doi.org/10.1371/journal.pone.0065555.
- Bink, D.I., Ritz, K., Aronica, E., van der Weerd, L., and Daemen, M.J.A.P. (2013). Mouse models to study the effect of cardiovascular risk factors on brain structure and cognition. J. Cerebr. Blood Flow Metabol. 33, 1666–1684. https://doi.org/10.1038/jcbfm.2013.140.
- 85. Yamamoto, M., Carrillo, J., Insunza, A., Mari, G., and Ville, Y. (2006). Error introduced into velocity measurements by inappropriate Doppler angle



- assignment. Ultrasound Obstet. Gynecol. 28, 853–854. https://doi.org/10.1002/uog.3847.
- Hartley, C.J., Reddy, A.K., Madala, S., Michael, L.H., Entman, M.L., and Taffet, G.E. (2007). Effects of isoflurane on coronary blood flow velocity in young, old and ApoE(-/-) mice measured by Doppler ultrasound. Ultrasound Med. Biol. 33, 512–521. https://doi.org/10.1016/j.ultrasmedbio. 2006.11.002.
- Liu, Z., Wang, Y., Kabraji, S., Xie, S., Pan, P., Liu, Z., Ni, J., and Zhao, J.J. (2019). Improving orthotopic mouse models of patient-derived breast cancer brain metastases by a modified intracarotid injection method. Sci. Rep. 9, 622. https://doi.org/10.1038/s41598-018-36874-3.
- 88. Hartley, C.J., Taffet, G.E., Michael, L.H., Pham, T.T., and Entman, M.L. (1997). Noninvasive determination of pulse-wave velocity in mice. Am. J. Physiol. *273*, H494–H500.





### **STAR**\*METHODS

#### **KEY RESOURCES TABLE**

REAGENT or RESOURCE	SOURCE	IDENTIFIER	
Chemicals, peptides, and recombinant proteins			
Sodium Nitroprusside (SNP)	Sigma-Aldrich, Inc.	13755-38-9	
Isoflurane	Sigma-Aldrich, Inc.	26675-46-7	
VivoVist <sup>™</sup> 0.25ML	Nanoprobes, Inc.	#1301-5X0.25ML	
Vascupaint Silicone Rubber Injection Compounds	MediLumine Inc	SKU: MDL-121	
Spectra 360 Electrode Gel	Parker Laboratories	#12-02	
HONEYWELL Single Use Eyewash Bottle	WW. Grainger, Inc.	#3ARE1	
Systane Night	McKesson	https://systane.myalcon.com/products/ systane-nighttime/	
PBS, Phosphate Buffered Saline, 10X Solution	Fisher Scientific	BP399500	
Experimental models: Organisms/strains			
BALB/C mice	Jackson Laboratory	IMSR_JAX:000651	
C57BL/6 J males/females	Jackson Laboratory	IMSR_JAX:000664	
Software and algorithms			
Ultrasound-based Doppler flow velocity measurement system software	Indus Instruments	https://indusinstruments.com/products/doppler-flow-velocity-system/(DSPW)	
Horos v4.0.0	the Horos Project	horosproject.org	
NRecon	Bruker Nano Analytics	https://www.bruker.com/en/products-and- solutions/preclinical-imaging/micro-ct/ skyscan-1276	
CTVOX	Bruker Nano Analytics	https://www.bruker.com/en/products-and- solutions/preclinical-imaging/micro-ct/ skyscan-1276	
Other			
Ultrasound-based Doppler flow Velocity measurement system	Indus Instruments	https://indusinstruments.com/products/doppler-flow-velocity-system/(DFVS)	
Micromanipulator	National Aperture	MM-3CR-XYZ	
The Bruker SkyScan 1276 CMOS edition	Bruker Nano Analytics	https://www.bruker.com/en/products-and solutions/preclinical-imaging/micro-ct/ skyscan-1276	
Mouse monitor	Indus Instruments	https://indusinstruments.com/products/ rodent-surgical-monitor (Mouse Monitor S	
CODA Monitor Single Channel noninvasive BP system	Kent scientific corporation	https://www.kentscientific.com/products/coda-monitor	

### **EXPERIMENTAL MODEL AND STUDY PARTICIPANT DETAILS**

Six months-old BALB/C males (Jackson Laboratory, Maine) were used for needle micro CT experiment (n=2); the sequential surgical ECA and ICA occlusions (n=2) and the sequential surgical obstruction of common carotid arteries (n=5) experiments. Three month-old C57BL/6J males (n=10) and females (n=10) (Jackson Laboratory, Maine) mice were used in the experiment with SNP. Three months-old C57Bl/6J males (n=3) and females (n=3) were used for dynamic changes in systemic blood pressure. Same sex mice were randomly assigned to experimental groups. Animals were housed at normal conditions (average temperature of  $20^{\circ}$ C and a humidity level of 30%) on a 12-h light-dark cycle. Food and water were available *ad libitum*. All manipulations were approved by the Institutional Animal Welfare Committee (AWC) of the Center for Laboratory Animal Medicine and Care (CLAMC) of the University of Texas Health Science Center at Houston (UTHealth), TX, USA. Animal Protocols AWC-22-0026 (IS) and AWC-23-0052 (SPM). UTHealth utilizes the 8th edition of the Guide for the Care and Use of Laboratory Animals



(NRC 2011), Public Health Service Policy on Humane Care and Use of Laboratory Animals, and the Animal Welfare Act and Regulations (AWAR) as standards for animal care and use program. All sections of this report adhere to the ARRIVE Guidelines for reporting animal research.

#### **METHOD DETAILS**

### **Doppler signal detection in OphA using DFVS**

### Finding optimal probe position for detection of OphA Doppler signal

The principle of operation of the DFVS is described in great detail elsewhere. 7,19,88 Mice were anesthetized with 2.0% isoflurane in the induction chamber and then transferred to a heated electrocardiogram (ECG) board (Mouse Monitor S, Indus Instruments, Webster, TX). The continuous anesthesia was delivered via the nose cone. Mice were placed in prone position with paws gently taped to the ECG electrodes. A small amount of electrically conducting paste was applied to each paw before affixing it. To minimize motion artifact during injection, the injection needle with the reagent was inserted in the right lower part of the peritoneal cavity before the right hind paw was affixed to the board. The board temperature was electronically controlled to maintain the core body temperature of the mouse at 37°C. Mouse ECG was continually monitored. Common ophthalmic saline (HONEYWELL Single Use Eyewash, WW Grainger, Inc) was used for signal coupling and ophthalmic ointment for eye protection (Systane Night, McKesson). The probe was supported and maintained in position by a micromanipulator (MM3CR-XYZ, National Aperture, Salem, NH). Guided by the real-time display of the wave shape, the optimal position of the probe that provides the strongest signal for arterial blood flow was sought. Using the manipulator, the US probe was used to scan the surface of the eyeball. The position near the temporal cantus of the eye produced a wave tracing characteristic for arterial blood flow: rapidly increasing systolic peak followed by dichrotic notch (indicating end of the systolic phase) and a gradually decreasing diastolic phase. The US probe tip was positioned right behind the eyeball perpendicular to the curvature of the skull, 90° in saggital and  $\sim$ 40 $^{\circ}$  in itransverse planes. Signal amplitude and brightness quality of the waveform was optimized by small angular movements of the probe supported by the micromanipulator. Once optimal position was established, the probe was fixed in place by the micromanipulator, allowing for a stable baseline recording. The time to find the arterial signal and secure the probe for recording was typically less than 10 min. After injection of the desired reagent for the desired timeline and the recording of the Doppler waveforms, the probe was removed, isoflurane turned off, the mouse freed from restraint and allowed to regain consciousness on a warm plate. After complete recovery from anesthesia, each mouse was transferred to its cage. Blood flow velocity parameters for each time point were determined by analysis of 6 cardiac cycles. Waveforms were analyzed using the Ultrasoundbased Doppler flow velocity measurement system software (DSPW, Indus instruments, TX). Markers placed for each arterial waveform were:

FVS - Flow Velocity Start: This marker is placed where the velocity signal begins to increase from zero velocity.

PFV - Peak Flow Velocity: This marker is placed at the highest velocity point within a single cardiac cycle.

MFV - Minimum Flow Velocity: This marker is placed at the minimum velocity point within a single cardiac cycle.

The obtained blood flow velocity waveform was used to extract several parameters, including peak, mean, and minimum flow velocities. Regional cerebral impedance could be also calculated using the angle independent pulsatility index (PI=(Vpeak-Vmin)/Vmean) and resistivity index (RI=(Vpeak-Vmin)/Vpeak).<sup>29</sup>

### Assessment of SNP response with DFVS

Using DFVS we assessed changes in peak blood flow velocity in mouse OphA in response to conventional vasodilator SNP. C57BL/6J male and female mice (Jackson Laboratories, Maine) were injected intraperitoneally (IP) with SNP (Sigma-Aldrich, 1 mg/kg dose) solution (5 males or 5 females) or PBS control (5 males and 5 females). Bolus volume was determined for each animal individually based on the weight. Once optimal probe position was achieved and the probe fixed in position, two baseline waveforms were acquired (1 min apart) before injection to establish baseline flow velocity. Time point acquisitions started with the injection time and were acquired every 15 sec for the first 2 min post-injection, followed by 1-min intervals (until 5 min post-injection), and then at 8, 10 and 15, 20 and 25 min. The time course was optimized experimentally for the comprehensive characterization of the kinetic response. Blood flow velocity parameters for each time point were determined by analysis of 6 cardiac cycles. The isoflurane flow was turned off 25 min after injection. Mice were then freed from restraint and allowed to regain consciousness on a warm plate. After complete recovery from anesthesia, each mouse was transferred to its cage.

### Recording systemic BP after SNP injection

Changes in systemic blood pressure was recorded using the non-invasive CODA tail-cuff system (Kent Scinetific, Co), according to a standard manufacturer's protocol. Briefly, C57Bl6/6J mice (n = 3 males, n = 3 females) were anesthetized by isoflurane and placed in a prone position on a heating pad. The occlusion and VPR cuffs were placed close to the base of the tail and connected to the CODA system. Once the baseline blood pressure value was stable, the mice were delivered an intraperitoneal bolus of sodium nitroprusside to achieve the dose of 1 mg/kg. The changes in blood pressure were recorded every 45 s for 1 h after nitroprusside administration.

### Sequential surgical obstruction of CCAs

A conventional approach to bilateral common carotid artery occlusion as in<sup>34</sup> was applied in our studies. Anesthetized mice were placed in supine position with 4 paws taped to ECG electrodes on a heated platform. After surgical procedure to



isolate the left and right carotid arteries, each artery was ensnared with sutures. A 6.0 silk suture with both ends passed through a 1mm PE10 tube (occlude) was placed around each artery. Next, the Doppler probe was positioned to a temporal canthus of the mouse left eye and a stable arterial blood flow signal was established after which, the probe was fixed in position by the micromanipulator. Steady baseline OphA flow was established and maintained for each animal for 1 min with both carotid arteries open. The suture snare ends for the right carotid artery were gently pulled apart until complete occlusion was achieved (RCc). OphA blood flow was allowed to stabilize for 1 min before the left carotid artery was occluded in a similar manner (LCc). Complete interruption of carotid blood flow was maintained for 3 s, followed by the release of the suture around the left carotid artery (LCo). The right carotid occlusion was opened (RCo) after 1 min to restore the OphA blood flow to baseline levels.

### **Ophthalmic artery identification**

### Mouse preparation for microCT imaging

This step was aimed to determine the identity of the artery producing the signal. To define the target path of the ultrasound probe we used microCT imaging to map the location of a fiduciary needle placed along the path of the ultrasound probe. The ultrasound probe was positioned to the temporal cantus of the mouse eye to obtain the characteristic Doppler signal of our targeted artery. Next, the mouse was overdosed on isoflurane (death was confirmed by flatline ECG) and a 25G stainless steel needle was inserted as a fiduciary along the path of the ultrasound probe (following the cylinder surface closest to the eye) to a 0.5 cm depth mimicking the reach of the US signal. The position of the registration needle was further secured by a drop of wax on the eye surface. The mouse was immediately transferred to the MicroCT Imaging Facility and the entire head was 3D imaged first with the fiduciary marker and then immediately after carefully removing the marker. MicroCT imaging was performed with a Bruker SkyScan 1276 imaging system. Imaging was performed with an X-ray source voltage of 70kV and 200 μA and using a 1 mm aluminum filter. A total of 450 projection images were acquired (360° rotation) at a final pixel resolution of 37 μm. 3D reconstructions were performed with Bruker NRecon and viewed by CTvol. The needle location was mapped to skull anatomical features. These coordinates were then used to extrapolate the location of the probe to the 3D scan of another mouse, which had been perfused with Vascupaint to provide CT imaging of the arterial vasculature. The anesthetized mouse was transcardially perfused with a vascular contrast agent, Vascupaint, a silicone-based ex vivo CT contrast agent that provides imaging of the arterial and arteriolar system (Medilumine; Montreal, Canada). The head of the Vascupaint-perfused mouse was imaged with the SkyScan 1276 system using X-ray source voltage of 70 kV and 200 μA and using a 1 mm aluminum filter. A total of 1200 projection images were acquired (360° rotation) at a final pixel resolution of 13 µm. 3D reconstruction and viewing was performed and images from both mice were overlapped and compared and analysis strongly indicate that the OphA is the source of acquired Doppler signal.

### In vivo microCT imaging with VivoVist

To visualize the intracranial and extracranial vasculature of the head and to confirm the targeted artery as the ophthalmic artery (OphA) and its origin from the ICA, *in vivo* microCT imaging of heads of two male BALB/c wild type mice (Jax Laboratories, Maine, IMSR\_JAX:000651) following intravenous delivery of 250  $\mu$ L of a blood pool contrast agent (VivoVist; Nanoprobes, Yaphank, NY). Imaging was performed under isoflurane anesthesia (1–1.5%) using the SkyScan 1276 instrument with an X-ray source voltage and current of 70 kV and 200  $\mu$ A and a 1 mm Aluminum filter. A total of 1200 projection images were acquired (360° rotation) at a final pixel resolution of 13  $\mu$ m. 3D reconstruction and viewing was performed as above and with Horos v4.0.0 (www.horosproject.org).

### Alternative surgical occlusion of ECA or ICA

This step is to provide functional confirmation of our anatomical findings. The surgical procedure was performed according to a previously described protocol adopted to our goals.<sup>87</sup> The mouse was anesthetized with 2% isoflurane was positioned on its back on a heated ECG pad and placed under a dissecting microscope. The fur was shaved from the neck area and the underlying skin was disinfected with antiseptic iodine solution. A midline, vertical, 1-cm skin incision was made, and the subcutaneous tissue, muscles and fat underwent blunt dissection using forceps to expose the left carotid sheath clearly visible under the microscope. The left CCA and branching site for ICA and ECA were identified and exposed by threading a 5.0 silk ligature underneath to separate from the surrounding nerves by gentle elevation of the CCA. Next, the Doppler probe was positioned to a temporal canthus of the mouse left eye and a stable arterial blood flow signal was established after which, the probe was fixed in position by the micromanipulator. After a baseline flow was acquired, the ECA and ICA snares were sequentially tightened for 3 s and then released. Doppler signal was recorded without interruption during sequential occlusions of the ICA and ECA. The procedure was repeated 3 times for each individual animal (total two mice were used).

### **QUANTIFICATION AND STATISTICAL ANALYSIS**

All experimental animals and samples were coded. SNP effects on OphA blood flow were done by an experimenter kept blind to the treatment schedule. The mice were randomly assigned to their groups using gender as the only criteria. Group sizes were optimized to use the least number of animals needed to yield less than 15% parameter variability while maintaining statistically



significant differences between groups. All datasets, both for SNP and carotid occlusion, have been tested and passed the test of normality by non-parametric Shapiro-Wilk test. Results are expressed as mean  $\pm$  Standard Deviation (St. Dev.). A paired 2-sided t-test was used for comparison between groups with p < 0.05 considered significant. A one-way ANOVA with post-hoc Tukey test was performed to compare female, male, and control groups against one another, yielding significant differences for all comparisons and a pooled variance of 34.85. The Q critical value for Control vs. female and Control vs. female groups was 9.85, which was less than the absolute mean differences of 38.62 and 25.02, respectively. The Q critical value for Male vs. Female groups was 8.99, which also was less than the absolute mean difference of 13.60.